Carbonization of polymers of intrinsic microporosity to microporous heterocarbon: Capacitive pH measurements

Naiara Hernandez [a], Jesus Iniesta [a], Vicente Montiel Leguey [a], Robert Armstrong [b], Stuart H. Taylor [b], Elena Madrid [c], Yuanyang Rong [c], Rémi Castaing [c], Richard Malpass-Evans [d], Mariolino Carta [d], Neil B. McKeown [d], Frank Marken [c,*]

[a] Departamento de Química física e Instituto Universitario de Electroquímica, Universidad de Alicante, Apartado 99, 03080 Alicante, Spain [b] School of Chemistry, Cardiff University, Main Building, Park Place, Cardiff CF10 3AT, UK
[c] Department of Chemistry, University of Bath, Claverton Down, Bath BA2 7AY, UK
[d] School of Chemistry, Joseph Black Building, David Brewster Road, University of Edinburgh, Edinburgh, Scotland EH9 3JF, UK

article info

Keywords:
Conformal carbonization
pH sensing
Micropore hydration
Voltammetry
Heterocarbon

abstract

A nitrogen-containing polymer of intrinsic microporosity (PIM-EA-TB-H_2 ; nitrogen adsorption surface area 846 $m^2\ g^{-1}$) is vacuum carbonized at 700 ° C and thereby directly without post-treatment converted into a microporous heterocarbon (cPIM; N_2 adsorption surface area 425 $m^2\ g^{-1}$). Nitrogen functional-ities in the polymer backbone are retained in the heterocarbon and appear responsible for unusual time-, electrolyte-, and pH-dependent properties. Electrochemical characterization suggests a high specific capacitance (typically 50 F g^{-1}) but only after prolonged immersion in aqueous $HClO_4$. The time-dependent increase in capacitance during immersion is assigned to slow hydration and ingress of $HClO_4$ into hydrophobic micropores (H_2SO_4 or H_3PO_4 are more hydrophilic and much less effective). Once hydrated, the microporous heterocarbon exhibits pH-dependent capacitance "switching" over a wide pH range and analytical applications as "capacitive" pH sensor are proposed.

1. Introduction

Novel carbon and nano-carbon materials provide an impor-tant driving force for the development of new (electro-)analytical methodology and sensor devices [1]. Particularly exciting are the recent development of "nano-dot" carbons [2], functionalized nanoparticles [3], the use of grafting to provide surface modified carbon sensors [4], hyper-crosslinked porous carbons [5], and the pyrolytic formation of microporous carbon substrates for electro-analysis [6].

Mesoporosity is considered to be crucial in sensor design [7] but less accessible microporosity in the <1 nm range may also provide selectivity in particular for smaller analytes, e.g. for protons (vide infra). Pyrolytically produced carbons [8], tailored microporous carbons [9], and metal-organic framework-based microporous het-erocarbons [10] are just some examples of a rapidly extending range of microporous heterocarbon materials now available to the analytical researcher. "Nitrogen-doped" heterocarbons and nanocarbons are of interest, for example, due to their catalytic prop-erties [11] or in sensing applications [12]. In this report we explore the properties of a microporous nitrogen-containing heterocarbon obtained via vacuum carbonization of a novel polymer of intrinsic microporosity, PIM-EA-TB-H_2 (see Fig. 1).

The measurement of pH (or proton activity) is routinely based on potentiometric (e.g. glass membrane with a pro-ton adsorption-dependent equilibrium potential) electrodes [13]. Although ubiquitous and fully established, these types of poten-tiometric pH measurements can be problematic when other adsorbing/surface active species are simultaneously present in the sample. This is particularly true in real biological samples, colloids, surfactant containing solutions, etc. It has therefore been suggested that amperometric sensors (e.g. based on the limiting current response of a microelectrode [14] or on dual-plate microtrench electrodes [15]) offer advantages for proton concentration deter-mination at least over limited proton concentration ranges. A new class of "reference-less" pH sensors based on the voltammetric response of pH-dependent surface redox systems has been devel-oped by Compton and coworkers based for example on quinone

* Corresponding author.
E-mail address: f.marken@bath.ac.uk (F. Marken).

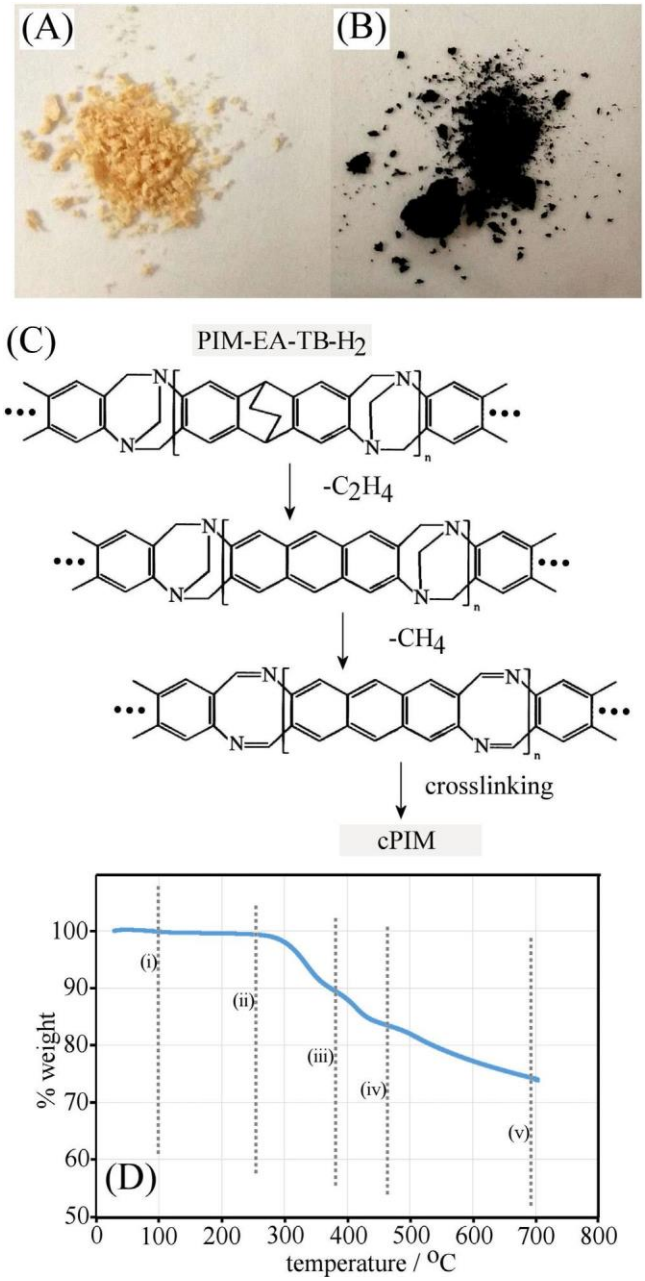

Fig. 1. (A and B) Photographic images for PIM-EA-TB-H_2 before and after vacuum carbonization. (C) Hypothetical reaction scheme to rationalize weight changes dur-ing carbonization. (D) Thermogravimetric analysis (TGA) data for PIM-EA-TB-H_2 under argon (see text).

functionalities grafted onto glassy carbon or graphite surfaces [16–20]. Other types of pH sensor concepts have been proposed, for example a pH-dependent impedance response was reported for aligned single walled carbon nanotubes [21]. Carbon compos-ite materials are often employed in sensor development [22] and a review has appeared summarizing pH sensing carbon materials and composites [23]. For most voltammetric pH sensor systems the measurement of a voltammetric current response is linked to a potential read out (relative to an internal standard) to give the pH reading. The use of a purely capacitive current signal (reported here) based on the charging/discharging currents (although briefly mentioned previously for core–shell carbon nanoparticle systems [24]) appears to be new and potentially very robust (there is no need for potential control) and there are opportunities for simple nano-sensor device concepts.

Pyrolysis of polymer precursors provides versatile access to both non-porous and porous electrode materials [6]. High quality sensor films can be produced for example from thin films of photo-resist polymer coatings [25,26]. Only recently has the carbonization of a polymer of intrinsic microporosity (PIM) been reported [27] to give interesting heterocarbon materials with both morphology and microporosity being retained during the carbonization process. This is in marked contrast to many other carbonization processes where post-treatments are applied to create/modify the desired microporosity. PIM materials [28] have emerged as a molecularly highly rigid polymer systems with the ability to absorb and sepa-rate gases [29], to sense gases [30], and they are currently under intense investigation for applications in electrochemistry [31].

The vacuum carbonization of PIM-EA-TB (a polymer of intrinsic microporosity – PIM – with ethano-anthracene – EA – structural components and Tröger base – TB – functionality [26]) at 500 °C was shown to yield electrically conducting carbon materials with-out change in shape, morphology, or in cumulative pore volume. It was recognized that the rigid molecular structure allows cross-linking with loss of some small molecular components, but without significant changes in polymer backbone and in morphology. In a follow-up study $PtCl_6^{2-}$ was adsorbed into the PIM-EA-TB pre-cursor and in a "one-step" vacuum carbonization a heterocarbon with embedded platinum nanoparticles was obtained [32]. Due to the rigid molecular structure, the size range of the resulting plat-inum nanoparticles was uniform and the surface of platinum was "free" of capping agents, and although encapsulated, immediately highly reactive in electrocatalysis without further pre-treatments. In another recent study on PIM carbonization, Kim et al. [33] have shown that also the prototypical polymer of intrinsic microporos-ity PIM-1 [34] can be carbonized (at 1100–1300 °C) to give thin microporous carbon membranes with improved ion rejection and flux properties for water purification under reverse osmosis condi-tions. Indeed, water flux and good salt rejection were reported to be better than those for current state-of-the-art water purification membranes.

In this study we explore the carbonization of PIM-EA-TB-H_2 (a polymer of intrinsic microporosity – PIM – with ethanoanthracene – EA – molecular motif linked via Tröger base – TB – function-ality: see structure in Fig. 1). This polymer is closely related to the previously reported polymer PIM-EA-TB [35], differing only in the lack of methyl groups at the bridgehead (9,10) position of the EA unit. PIM-EA-TB-H_2 is readily prepared in three simple steps from the cheaply prepared Diels–Alder adduct of ethylene and anthracene. A heterocarbon powder sample is obtained at 700 °C vacuum carbonization conditions and employed as ink applied to glassy carbon in electrochemical studies. Unique properties such as slow electrolyte-dependent hydration and pH-dependent capaci-tance responses are assigned to the presence of micropores and N-hetero atoms throughout the microporous carbon. Applications in "capacitive" pH sensing are suggested.

2. Experimental

2.1. Chemical reagents

All solutions were prepared with deionized water of resistiv-ity not less than 18.2 M cm^{-1} at 25 °C from a Thermo Scientific water purification system. Isopropanol, perchloric acid (70%), sul-furic acid (97%), phosphoric acid (85%), Nafion-117 solution (5% wt), sodium dihydrogenphosphate (99%) and sodium phosphate diba-sic heptahydrate were purchased from Sigma–Aldrich and used

without further purification. PIM-EA-TB-H_2 was obtained following a literature recipe [35].

Briefly, the synthesis of PIM-EA-TB-H_2 was performed by nitra-tion of the ethanoanthacene hydrocarbon, followed by reduction to give the required 2,6(7)-diaminoethanoanthracene monomer, which was readily polymerized by the action of dimethoxymethane in trifluoroacetic acid as previously reported for PIM-EA-TB [36].

2.2. Instrumentation

Electrochemical measurements were performed with a poten-tiostat system (IVIUM Compactstat) or a Autolab type III potentiostat/galvanostat controlled by Autolab GPES software ver-sion 4.9 for windows XP in a conventional three electrode cell, with a Pt wire as a counter electrode, a KCl-saturated calomel reference (SCE, Radiometer, Copenhagen) as reference electrode, and a glassy carbon disk electrode (GC, BASi) with 3 mm diameter as working electrode. The heterocarbon powder was applied to the electrode as an ink (vide infra).

Morphologies of the PIM-EA-TB-H_2 before and after the car-bonization were analyzed with a JEOL SEM6480LV scanning electron microscopy (SEM). Raman spectroscopy was carried out on a Renishaw inVia system with = 785 nm excitation. Ther-mogravimetric analysis (TGA) data were collected on a Setaram Setsys Evolution TGA instrument under Ar from 20 $^{\circ}$ C to 700 $^{\circ}$ C. For nitrogen adsorption analysis, samples (ca. 0.025 g) were degassed (120 $^{\circ}$ C, 6 h) prior to analysis. Analyses were carried out (for three samples: (A) PIM-EA-TB-H_2 treated with aqueous 0.1 M HCl, rinsed and dried; (B) PIM-EA-TB-H_2 treated with aqueous 0.1 M NaOH, rinsed and dried; (C) carbonized PIM-EA-TB-H_2) at 77 K on a Micromeritics 3Flex with P_0 measured continuously. Free space was measured post- analysis with He. Using nitrogen as the adsor-bate gas at 77 K, an 80 point physisorption analysis was undertaken and the data analyzed by the DFT method (N_2 at 77 K, cylindrical pore, NLDFT equilibrium model).

Elemental analysis (obtained by Butterworth Laboratories Ltd., London in triplicate) suggest for sample (A) PIM-EA-TB-H_2 treated with aqueous 0.1 M HCl, rinsed and dried C 75.50% H 6.15% N 9.47%; sample (B) PIM-EA-TB-H_2 treated with aqueous 0.1 M NaOH, rinsed and dried C 77.61% H 6.01% N 9.78%; and sample (C) carbonized PIM-EA-TB-H_2 C 83.19% H 2.46% N 5.67%.

2.3. Procedure for electrode preparation

Carbonization of the PIM-EA-TB-H_2 powder was performed at 700 $^{\circ}$ C for 3 h under vacuum (Edwards oil pump at ca. 4 mbar) in a custom-made quartz tube employing an Elite Thermal Systems Ltd. oven. An amount of 2 mg of the black powder (cPIM) obtained from the PIM-EA-TB-H_2 carbonization and 100 L of 0.25 wt% Nafion solution were ground together (mortar and pestle) and dispersed in 1 mL of isopropanol. The resulting ink was dispersed by sonica-tion for 15 min to form a homogeneous ink. Different amounts of the ink (typically 3 L = 5.5 g cPIM carbon) were placed onto the 3 mm diameter glassy carbon disk electrode (GC, BASi) and dried under ambient conditions.

3. Results and discussion

3.1. Characterization of carbonized polymer of intrinsic microporosity (cPIM)

The polymer PIM-EA-TB-H_2 is obtained as a pale-yellow pow-der and when vacuum carbonized at 700 $^{\circ}$ C a black hetero-carbon is obtained (see Fig. 1A and B). Based on the elemental CHN analy-sis (see Section 2) the highly porous polymer before carbonization is likely to contain captured guest molecules, which lead to some deviation from the ideal calculated elemental mass C 83.8% H 5.9% N 10.3%. In particular, uptake of acids such as HCl lead to a decrease in carbon (C 75.50% H 6.15% N 9.47%), but there is clear evidence for the presence of nitrogen. A treatment with aqueous 0.1 M NaOH followed by rinsing and drying changes the compo-sition analysis (C 77.61% H 6.01% N 9.78%) indicative of removal of at least some of the guest species. The vacuum carbonization to give cPIM increases the carbon content (C 83.89% H 2.46% N 5.67%) and decreases the hydrogen content. The nitrogen content is lowered, but mainly retained, indicative of a polymer back bone staying intact. Data from thermo-gravimetric analysis (Fig. 1D) shows that a minor release of water occurs around 100 $^{\circ}$ C (i) and the release of small structural components (e.g. ethylene from a retro-Diels–Alder reaction) occurs in the range 250–350 $^{\circ}$ C (ii) with onset of carbonization occurring from 380 $^{\circ}$ C (iii) to 460 $^{\circ}$ C (iv) with a final weight loss of approximately 25% at 700 $^{\circ}$ C. A hypothetical reaction scheme [27] is shown in Fig. 1C suggesting some cross-linking as the carbonization progresses. Details of the carbonization chemistry are complex and temperature-/time-dependent and therefore the reaction scheme in Fig. 1C is speculative. However, most of the poly-mer backbone material is suggested to remain structurally intact to give a porous nitrogen-containing hetero carbon without chemical post-treatment with interesting implications for application of the heterocarbon.

Analysis of Raman data (Fig. 2A and B) suggests that at an excitation wave length of 785 nm some fluorescence occurs in the background for the PIM-EA-TB-H_2 spectra, which are oth-erwise dominated by spectral lines at 800 cm^{-1} and 1350 cm^{-1} similar to those seen for PIM-EA-TB [27]. After 700 $^{\circ}$ C vacuum car-bonization only the prominent Raman peaks for graphitic materials (no fluorescence) are observed at 1329 cm^{-1} (D-peak, disordered amorphous carbon) and at 1594 cm^{-1} (G-peak, graphitic carbon) [37]. The D-peak seems to be composed of overlapping peaks. Fur-ther deconvolution of the Raman spectra for cPIM shows that four Gaussian-shaped bands are present: G and D bands at 1329 cm^{-1} and 1594 cm^{-1} , a shoulder present at the left of the D band at 1178 cm^{-1} due to the TPA band (related to trans-polyacetylene-like structures, [38,39]) and the A band at 1512 cm^{-1} , which contributes to the intensity between G and D band and which is observed in other types of disordered carbons [32]. However, the D band, which is related to defect-induced breaking of translational symmetry, is not present in the spectra. There is also very little evidence for the 2D peak usually seen at 2770 cm^{-1} for graphitic or carbon nan-otube materials. The intensity ratio I_D/I_G = 1.17 is consistent with a high level of defects and some similarity of the spectrum exists in particular with glassy carbon materials [40].

Scanning electron microscopy images of the morphology of the polymer starting material (PIM-EA-TB-H_2) and of the product after 700 $^{\circ}$ C vacuum carbonization (cPIM) are shown in Fig. 2C–F. Fig. 2C and D are obtained at lower magnification and Fig. 2E and F shows the morphology for the polymer precursor and for the cPIM prod-uct at higher magnification. As reported recently for a related PIM material [27], due to retention of the structural backbone there is very little change in morphology upon vacuum carbonization.

In order to obtain further insight into the micropore struc-ture powder samples were investigated with nitrogen adsorption methods (BET) before and after carbonization. Fig. 3A shows a comparison of isotherms comparing PIM-EA-TB-H_2 (i) treated with aqueous 0.1 M HCl (causing some swelling and protonation [41]),
(ii) treated with aqueous 0.1 M NaOH (to remove unwanted protons and impurities; BET data for “as synthesized” PIM-EA-TB-H_2 are not shown but were similar to those for NaOH treated material), and
(iii) a sample after vacuum carbonization. After carbonization nitro-gen gas adsorption is lowered. The BET surface area (see Fig. 3B) is reduced from 846 $m^2\ g^{-1}$ for pure PIM-EA-TB-H_2 (somewhat lower when compared to PIM-EA-TB [27,40]) to 425 $m^2\ g^{-1}$ for cPIM. DFT

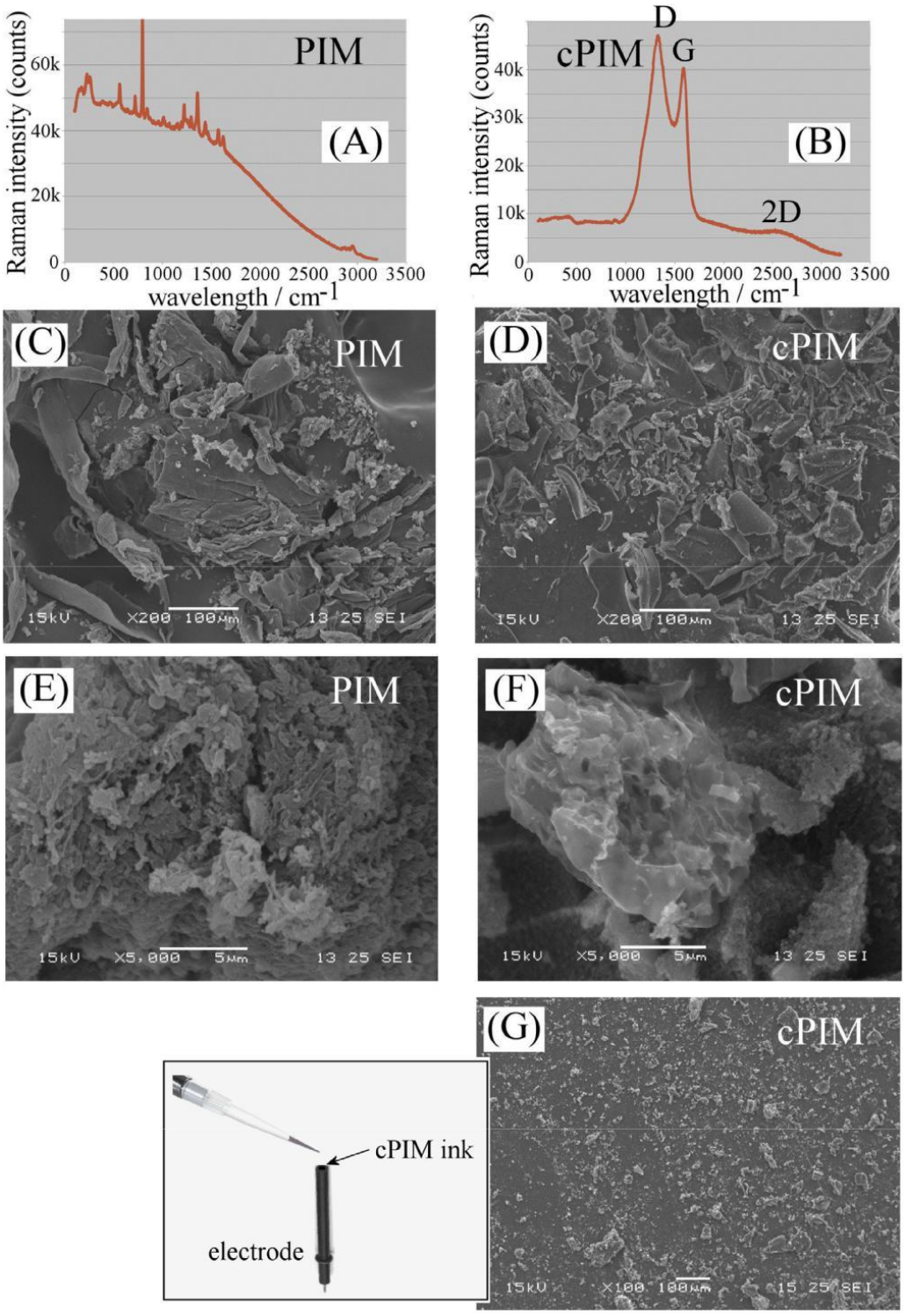

Fig. 2. (A and B) Raman spectra obtained with = 785 nm for PIM and cPIM materials. (C and E) Scanning electron microscopy (SEM) images for PIM at low and at high magnification. (D and F) SEM images for cPIM at low and at high magnification. (G) SEM image for the cPIM ink (3 L = 5.5 g carbon) applied to the 3 mm diameter glassy carbon electrode.

analysis of the pore size distribution (Fig. 3C and D) suggests that changes in cumulative pore volume due to vacuum carbonization are relatively small (when compared to changes induced by pro-tonation), which is in agreement with previous observations with a related polymer, suggesting only minor changes in morphology. A significant loss of very small micropores appears to occur upon carbonization, which could be due to cross-linking and loss of flex-ibility in the polymer chains.

3.2. Electrochemical properties of carbonized polymer of intrinsic microporosity I: time effect and capacitance

In order to investigate the electrochemical properties of the car-bonized material, cPIM, an ink based on isopropanol, 0.023 wt% Nafion (or 0.23 g/ L), and cPIM (1.8 g/ L) was prepared and applied to 3 mm diameter glassy carbon substrate electrodes. Typ-ically a 3 L volume of ink was deposited to give approximately

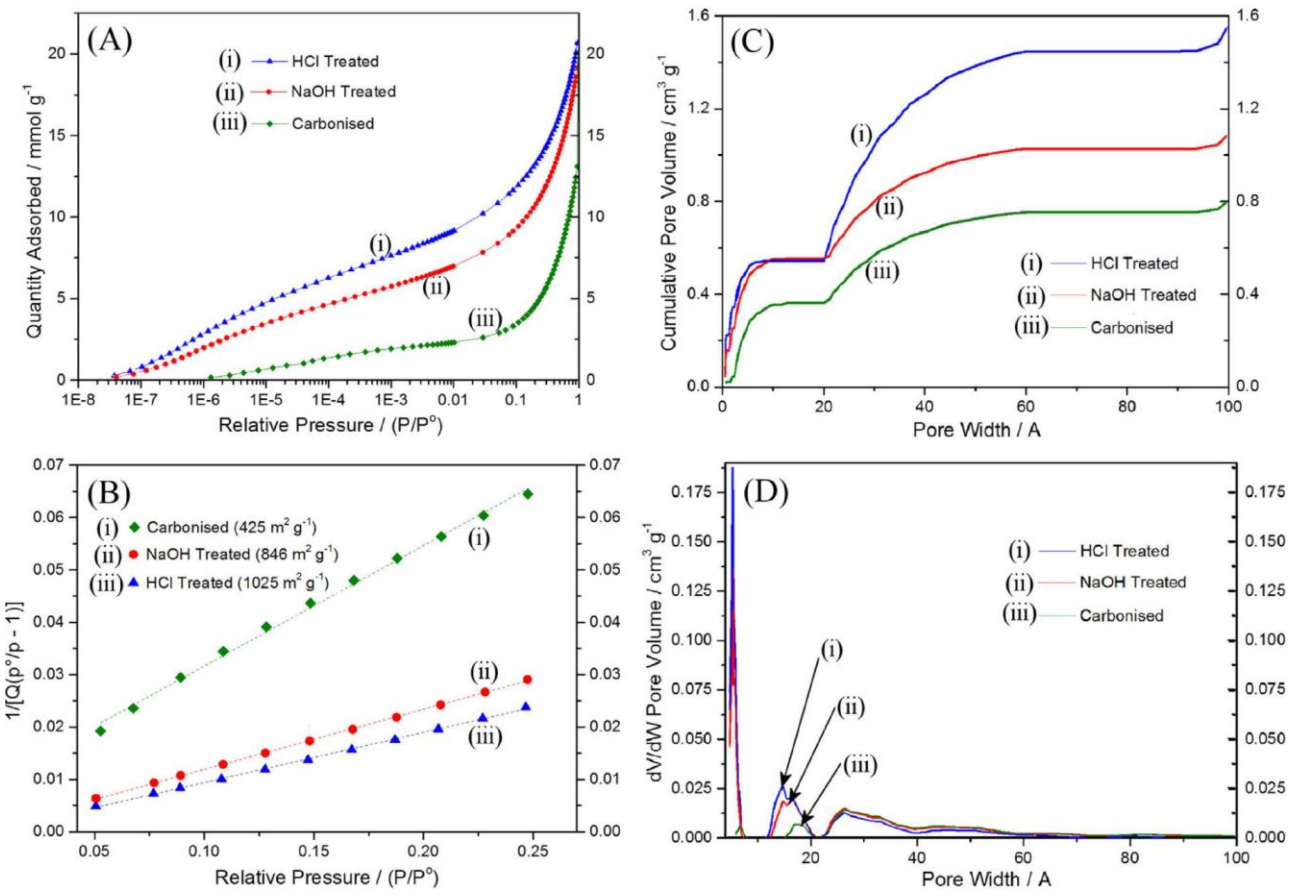

Fig. 3. (A) Nitrogen adsorption isotherms (BET) for (i) PIM-EA-TB-H_2 HCl treated, (ii) PIM-EA-TB-H_2 NaOH treated, and (iii) PIM-EA-TB-H2 vacuum carbonized. (B) BET analysis plots and surface area. (C) Cumulative pore volume and (D) pore volume analysis (DFT method, N_2 at 77 K, cylindrical pore, NLDFT equilibrium model).

5.5 g cPIM deposit (see SEM image in Fig. 2G). When immersed into aqueous 0.1 M $HClO_4$ and when employing cyclic voltamme-try (see Fig. 4A) an increase in capacitance is immediately observed upon immersion. However, gradually with time a much stronger increase in capacitance was noted. The value for the capacitance is estimated here from the capacitive background current at 0.25 V vs. SCE in the cyclic voltammogram based on specific capaci-tance = I_{cap} /(scan rate × weight). Fig. 4C shows a plot of specific capacitance increasing over a period of 24 h. This gradual increase is assigned here to a gradual penetration of protons and hydration into the microporous heterocarbon interior. Carbon particles are not uniformly sized (see Fig. 2G) and in particular bigger particles may contribute to this effect more significantly.

The effect of scan rate on the voltammetric response (Fig. 4B) is consistent with that for a capacitive current signal with approx-imately linear increase of current with scan rate. In order to investigate the effects of the amount of ink deposit, experiments were repeated with a scan rate of 5 mV s^{-1} for (i) 2.8, (ii) 5.5, (iii) 9.1, (iv) 12.7, (v) 16.4 g cPIM ink on a 3 mm diameter glassy carbon electrode (see Fig. 4D and E). The specific capacitance after 24 h sub-mersion appeared reproducible up to approximately 10 g cPIM ink deposit, but beyond this thickness a decrease is observed possi-bly linked to insufficient inter-particle conductivity in thicker film deposits. Therefore, experiments were performed with less than 10 g cPIM loading.

The slow increase in specific capacitance appeared to be linked to gradual hydration/protonation of the cPIM heterocarbon par-ticles and additional experiments were performed exploring the effect of the electrolyte on this wetting process. Initial experiments in Fig. 4 were performed in 0.1 M $HClO_4$ and in Fig. 5 shows data for (A) 1 M $HClO_4$, (B) 1 M H_2SO_4 , and (C) 1 M H_3PO_4 electrolyte. The effect of the $HClO_4$ concentration on the hydration process appears insignificant, but the effect of the electrolyte anion is pronounced.

When comparing data for $HClO_4$ and H_2SO_4 , the perchloric acid solution appears to hydrate the cPIM much more rapidly. In con-trast H_3PO_4 shows very little increase, even after long immersion periods. Additional experiments in non-acidic aqueous media sug-gest that acidic conditions are required for the specific capacitance to increase. Mechanistically, it can be suggested that protonation of nitrogen sites in the cPIM heterocarbon is involved in the inter-nal wetting process. This is coupled to uptake of anions into small micropores and cavities. Strongly hydrated anions such as SO_4^{2-} or PO_4^{3-} are detrimental in this case, but the weakly hydrated per-chlorate anion may be much more suited to bind into hydrophobic micropores and drive the internal uptake of electrolyte and water into cPIM micropores. Porosity effects in the cPIM material elec-trochemistry appear to be dominated by very small pores and by ingress of protons into deeper regions of the heterocarbon material. This effect was not observed for cPIM obtained from PIM-EA-TB [27] and is likely to be linked to the higher carbonization temperature, here 700 ° C compared to previously 500 ° C [27].

It is interesting to ask whether the hydration is permanent and whether a change in pH can reversibly or irreversibly change the specific capacitance of the cPIM material. In Fig. 5E data for an experiment based on switching the pH is shown. A glassy carbon electrode was coated with 5.5 g cPIM and then initially immersed into aqueous 0.1 M $HClO_4$ for 12 h. The specific capacitance reaches 55 F g^{-1} . When immersed into aqueous 0.1 M phosphate buffer pH 7 the capacitance immediately drops by an order of magnitude. Per-haps surprisingly, the capacitance is immediately switched back

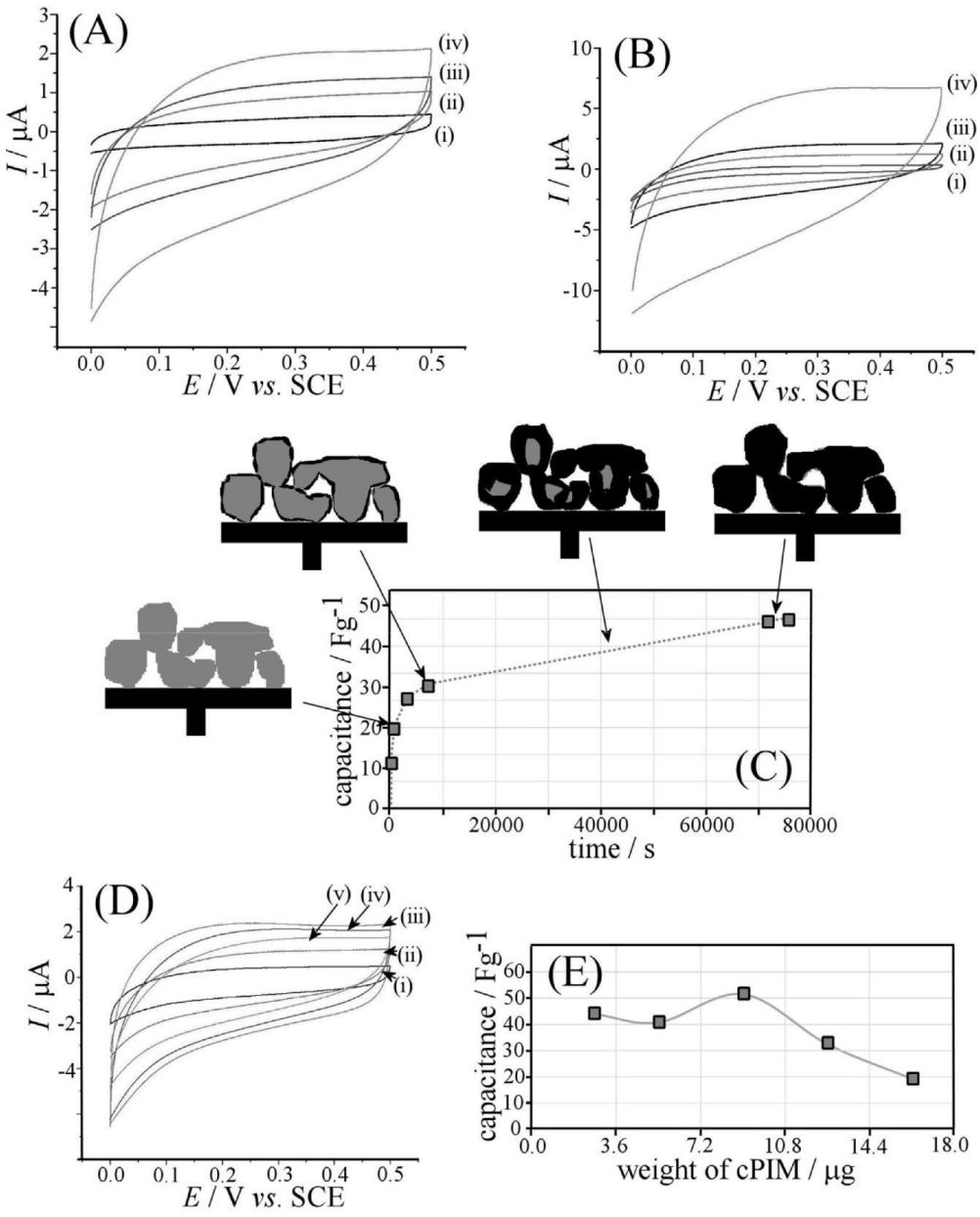

Fig. 4. (A) Cyclic voltammograms (10 mV s^{-1} , third cycle) for cPIM (5.5 g deposited onto a 3 mm diameter glassy carbon electrode) immersed in aqueous 0.1 M $HClO_4$. The influence of the time submerged in solution on the voltammetric response is shown for (i) bare glassy carbon background, (ii) 5 min, (iii) 1 h, and (iv) 12 h. (B) Cyclic voltammograms (scan rate (i) 1 mV s^{-1} , (ii) 5 mV s^{-1} , (iii) 10 mV s^{-1} , and (iv) 50 mV s^{-1}) for a 24 h submerged 5.5 g cPIM coated electrode. (C) Plot of the specific capacitance (estimated from cyclic voltammograms) vs. submersion time. (D) Cyclic voltammograms (scan rate 5 mV s^{-1}) for (i) 2.8 g, (ii) 5.5 g, (iii) 9.1 g, (iv) 12.7 g, and (v) 16.4 g cPIM deposited onto a 3 mm diameter glassy carbon electrode and immersed into 0.1 M $HClO_4$. (E) Plot of apparent specific capacitance vs. amount of cPIM deposit.

"on" by re-immersion into 0.1 M $HClO_4$ (Fig. 5E). Therefore the internal hydration appears to be retained even if H^+ and ClO_4^- ions are removed (Fig. 5F). This switching process is reversible and an equilibration time of approximately 5 min appeared suf-ficient for a stable capacitance response reading to be obtained. This suggests that the state of protonation of the microporous cPIM material quickly responds to external pH conditions and with the change in internal protonation the specific capacitance dramati-cally changes even when the state of hydration is not changing. The internal protonation appears to be linked to an apparent increase in the capacitive surface area as indicated schematically in Fig. 5F. A potential application of this phenomenon is envisaged in "non-potentiometric" pH sensing.

3.3. Electrochemical properties of carbonized polymer of intrinsic microporosity II: pH effects

In order to further explore the effects of pH, electrochemical impedance experiments were performed. A glassy carbon electrode loaded with 5.5 g cPIM and pre-immersed into aqueous 0.1 M $HClO_4$ solution is employed. The electrode is kept in 0.1 $HClO_4$ and only for measurements transferred into aqueous 0.1 M phosphate buffer media. Fig. 6A shows impedance data obtained at 0.25 V vs. SCE for a frequency range from 10 kHz to 0.1 Hz represented as Nyquist plots. An approximate equivalent circuit model to fit the data was based on an external resistance R, in series with a Warburg diffusion element to account qualitatively for internal ion and charge diffusion, and a series capacitance C to account for the

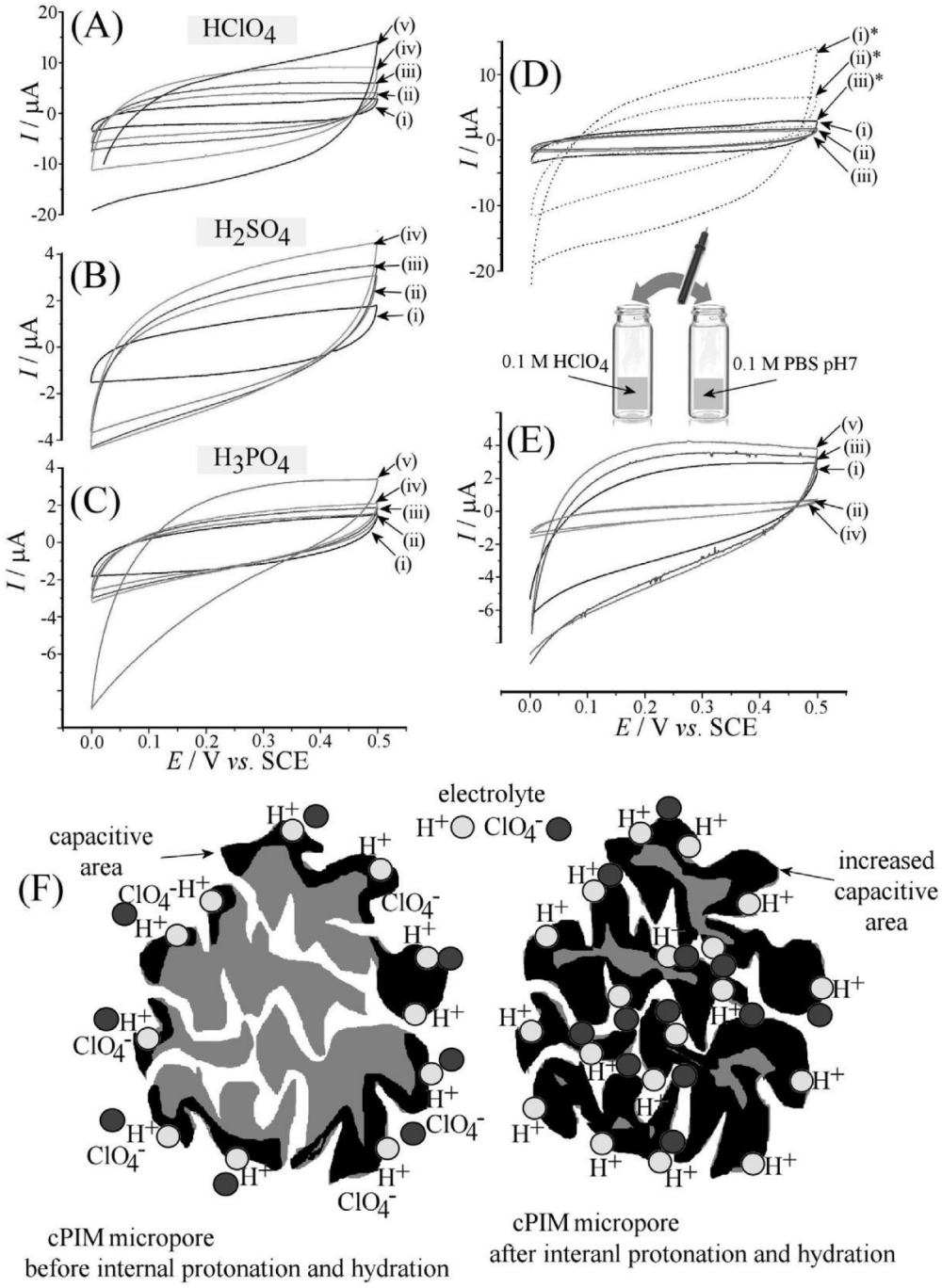

Fig. 5. Cyclic voltammograms (scan rate 50 mV s^{-1}) for 5.5 g cPIM on glassy carbon immersed for (i) bare glassy carbon background, (ii) 2 min, (iii) 10 min, (iv) 1 h, and (v) 12 h in (A) 1 M $HClO_4$, (B) 1 M H_2SO_4 , and (C) 1 M H_3PO_4 . (D) Comparison of cyclic voltammograms (scan rate 50 mV s^{-1} , solid bare glassy carbon, dotted 5.5 g cPIM) immersed 12 h in (i) $HClO_4$, (ii) H_2SO_4 , and (iii) H_3PO_4 . (E) Cyclic voltammograms (scan rate 10 mV s^{-1}) for 5.5 g cPIM immersed 12 h in 0.1 M $HClO_4$ and then immersed (for 5 min each) sequentially in (i) 0.1 M $HClO_4$, (ii) 0.1 M phosphate buffer pH 7, (iii) 0.1 M $HClO_4$, (iv) 0.1 M phosphate buffer pH 7, and (v) 0.1 M $HClO_4$. (F) Schematic drawing to illustrate internal protonation and wetting of cPIM micropores.

charging of the cPIM heterocarbon material. Data extracted for R and for C are shown in Fig. 6B and C, respectively.

The series resistance shows an almost linear correlation to pH over a pH 4 to pH 12 range. The capacitance C appears independent of pH in the alkaline range, but then rapidly increases in the acidic pH range. At pH 2 the specific capacitance is estimated 70 F g^{-1} with further increase in the acidic range probably leading to super capacitor performance. It is interesting to combine R and C into the characteristic frequency $(RC)^{-1}$ as shown plotted vs. pH in Fig. 6D.

Again, a close to linear correlation with pH over a broad range of pH values is observed.

This “capacitive” pH reading is likely to be insensitive to col-loid and surfactant adsorption and other interference which affect potentiometry. The application of a capacitive current response (capacitive pH sensor) based on the internal micropore protonation of cPIM particles could be robust and versatile and further study of this material is in progress. The properties of the cPIM material as well as the sensor architecture need to be further developed and

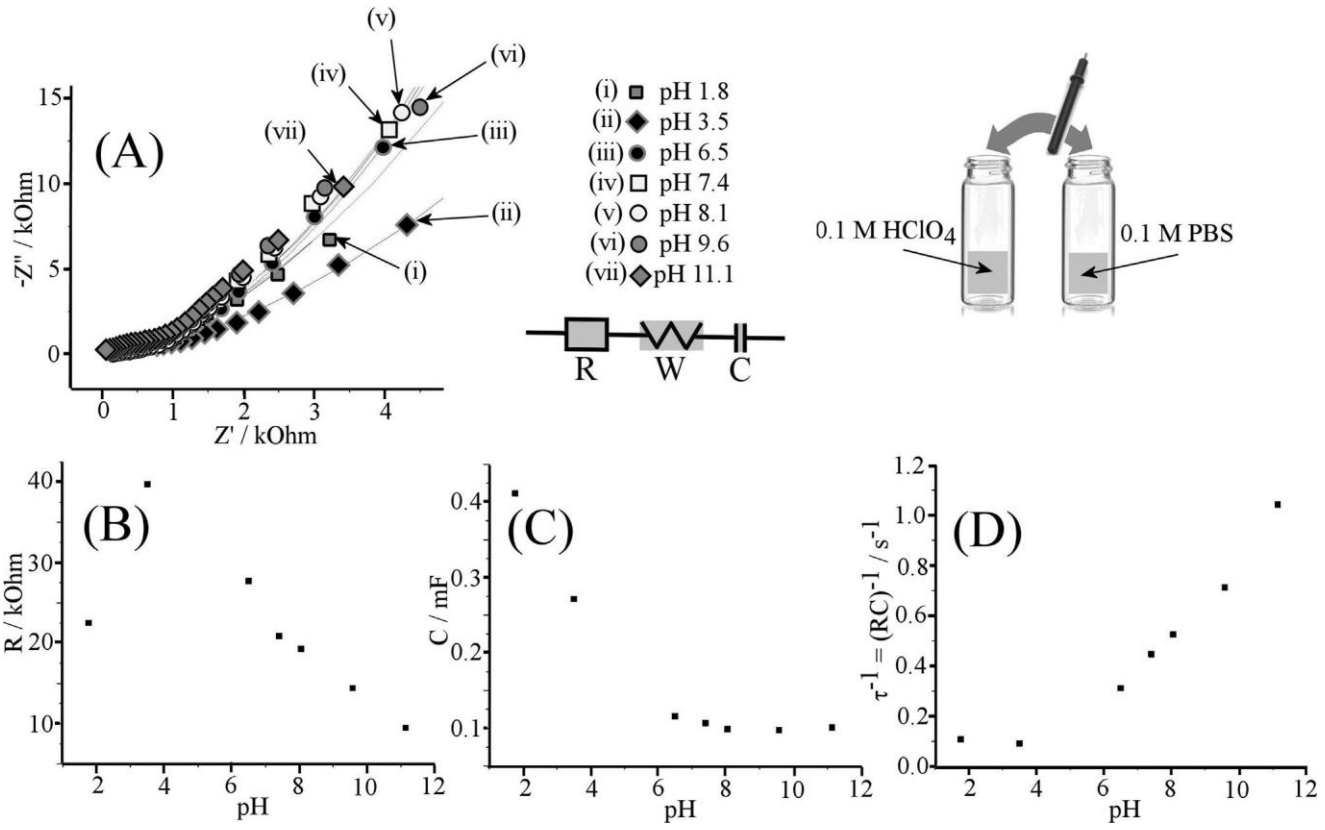

Fig. 6. (A) Nyquist plots for impedance measurements (10 kHz to 0.1 Hz, 50 mV amplitude) for 5.5 g cPIM on glassy carbon immersed for 2 min in 0.1 M phosphate buffer at various pH values. Before the measurement (12 h) and in between measurements the electrode was immersed in 0.1 M $HClO_4$. Lines indicates fits for a simple RWC model.
(B) Plot of the resistance R vs. pH. (C) Plot of the capacitance C vs. pH. (D) Plot of the inverse time constant $(RC)^{-1}$ vs. pH.

optimized to be capable to work for example in complex media such as wound dressings.

4. Conclusion

It has been shown that the vacuum carbonization of the polymer of intrinsic microporosity PIM-EA-TB-H_2 yields a novel microp-orous heterocarbon with properties very closely related to those of the starting polymer. The polymer backbone and porosity are maintained. Nitrogen in the molecular structure is retained (in part) during the 700 ° C carbonization process and protonation of nitrogen in micropores has been suggested to be responsible for unusual phenomena such as a slow electrolyte dependent hydra-tion process and a “capacitive” pH response. The immersion time and pH-dependent capacitance has been explained with ingress of protons associated with electrolyte anions into micropores with the associated increase in the apparent capacitive surface area. The protonation/deprotonation processes appear to be fast when compared to the wetting/dewetting processes of micropores. In future this will allow a simple impedance-based pH probe to be constructed without the need for a reference electrode and with performance characteristics that are likely to be complementary (and applicable in complex media) to those of existing pH sensing equipment.

Acknowledgement

N.H. and J.I. thank MINICINN, Spain (projects CTQ2013-48280-C3-3-R and CTQ2016-76231-C2-2-R) for financial support and the University of Alicante for support for a PhD exchange visit. F.M. and N.B.M. thank the Leverhulme Foundation for financial support (RPG-2014-308: “New Materials for Ionic Diodes and Ionic Photo-diodes”).

References

[1] N.J. Yang, G.M. Swain, X. Jiang, Nanocarbon electrochemistry and electroanalysis: current status and future perspectives, Electroanalysis 28 (2016) 27–34.

[2] Y.L. Ying, X.S. Peng, Recent advances in carbon-based dots for electroanalysis, Analyst 141 (2016) 2619–2628.

[3] K. Lawrence, C.L. Baker, T.D. James, S.D. Bull, R. Lawrence, J.M. Mitchels, M. Opallo, O.A. Arotiba, K.I. Ozoemena, F. Marken, Functionalized carbon nanoparticles, blacks and soots as electron-transfer building blocks and conduits, Chem. Asian J. 9 (2014) 1226–1241.

[4] H. Randriamahazaka, J. Ghilane, Electrografting and controlled surface functionalization of carbon based surfaces for electroanalysis, Electroanalysis 28 (2016) 13–26.

[5] J.S.M. Lee, M.E. Briggs, T. Hasell, A.I. Cooper, Hyperporous carbons from hyper-crosslinked polymers, Adv. Mater. 28 (2016) 9804–9805.

[6] T.E. Benavidez, R. Martinez-Duarte, C.D. Garcia, Analytical methodologies using carbon substrates developed by pyrolysis, Anal. Methods 8 (2016) 4163–4176.

[7] A. Walcarius, Mesoporous materials-based electrochemical sensors, Electroanalysis 27 (2015) 1303–1340.

[8] K.J. Sun, Q. Yang, G.H. Zhao, H. Peng, G.F. Ma, Z.Q. Lei, Nitrogen-doped high surface area carbon as efficient electrode material for supercapacitors, Nano 11 (2016) 1650076.

[9] L. Borchardt, M. Oschatz, S. Kaskel, Tailoring porosity in carbon materials for supercapacitor applications, Mater. Horizons 1 (2014) 157–168.

[10] B. Ding, J. Wang, Z. Chang, G.Y. Xu, X.D. Hao, L.F. Shen, H. Dou, X.G. Zhang, Self-sacrificial template-directed synthesis of metal-organic framework-derived porous carbon for energy-storage devices, ChemElectroChem 3 (2016) 668–674.

[11] K.Y. Park, J.H. Jang, J.E. Hong, Y.U. Kwon, Mesoporous thin films of nitrogen-doped carbon with electrocatalytic properties, J. Phys. Chem. C 116 (2012) 16848–16853.

[12] S. Majeed, J.M. Zhao, L. Zhang, S. Anjum, Z.Y. Liu, G.B. Xu, Synthesis and electrochemical applications of nitrogen-doped carbon nanomaterials, Nanotechnol. Rev. 2 (2013) 615–635.

[13] F.G.K. Baucke, The glass-electrode – applied electrochemistry of glass surfaces, J. Non-Cryst. Solids 73 (1985) 215–231.
[14] J. Weber, A.J. Wain, F. Marken, Microwire chronoamperometric determination of concentration, diffusivity, and salinity for simultaneous oxygen and proton reduction, Electroanalysis 27 (2015) 1829–1835.
[15] S.E.C. Dale, A. Vuorema, M. Sillanpää, J. Weber, A.J. Wain, E.O. Barnes, R.G. Compton, F. Marken, Nano-litre proton/hydrogen titration in a dual-plate platinum–platinum generator-collector electrode micro-trench, Electrochim. Acta 125 (2014) 94–100.
[16] M. Lu, R.G. Compton, Voltammetric pH sensing using carbon electrodes: glassy carbon behaves similarly to EPPG, Analyst 139 (2014) 4599–4605.
[17] L.H.J. Xiong, C. Batchelor-McAuley, R.G. Compton, Calibration less pH sensors based on nitrosophenyl and ferrocenyl co-modified screen printed electrodes, Sens. Actuators B-Chem. 159 (2011) 251–255.
[18] N.S. Lawrence, M. Pagels, S.F.J. Hackett, S. McCormack, A. Meredith, T.G.J. Jones, G.G. Wildgoose, R.G. Compton, L. Jiang, Triple component carbon epoxy pH probe, Electroanalysis 19 (2007) 424–428.
[19] H.C. Leventis, I. Streeter, G.G. Wildgoose, N.S. Lawrence, L. Jiang, T.G.J. Jones, R.G. Compton, Derivatised carbon powder electrodes: reagentless pH sensors, Talanta 63 (2004) 1039–1051.
[20] G.G. Wildgoose, M. Pandurangappa, N.S. Lawrence, L. Jiang, T.G.I. Jones, R.G. Compton, Anthraquinone-derivatised carbon powder: reagentless voltammetric pH electrodes, Talanta 60 (2003) 887–893.
[21] U. Hashim, F.W. Low, W.W. Liu, Precise alignment of individual single-walled carbon nanotube using dielectrophoresis method for development and fabrication of pH sensor, J. Nanomater. (2013) 825285.
[22] M.M. Barsan, E.M. Pinto, M. Florescu, C.M.A. Brett, Development and characterization of a new conducting carbon composite electrode, Anal. Chim. Acta 635 (2009) 71–78.
[23] H. Kahlert, Functionalized carbon electrodes for pH determination, J. Solid State Electrochem. 12 (2008) 1255–1266.
[24] K. Lawrence, G.W. Nelson, J.S. Foord, M. Felipe-Sotelo, N.D.M. Evans, J.M. Mitchels, T.D. James, F.J. Xia, F. Marken, "Hydrothermal wrapping" with poly(4-vinylpyridine) introduces functionality: pH-sensitive core–shell carbon nanomaterials, J. Mater. Chem. A 1 (2013) 4559–4564.
[25] C. Fairman, S.S.C. Yu, G.Z. Liu, A.J. Downard, D.B. Hibbert, J.J. Gooding, Exploration of variables in the fabrication of pyrolysed photoresist, J. Solid State Electrochem. 12 (2008) 1357–1365.
[26] A.J. Gross, A.J. Downard, Regeneration of pyrolyzed photoresist film by heat treatment, Anal. Chem. 83 (2011) 2397–2402.
[27] Y.Y. Rong, D.P. He, A. Sanchez-Fernandez, C. Evans, K.J. Edler, R. Malpass-Evans, M. Carta, N.B. McKeown, T.J. Clarke, S.H. Taylor, A.J. Wain, J.M. Mitchels, F. Marken, Intrinsically microporous polymer retains porosity in vacuum thermolysis to electroactive heterocarbon, Langmuir 31 (2015) 12300–12306.
[28] N.B. McKeown, P.M. Budd, Exploitation of intrinsic microporosity in polymer-based materials, Macromolecules 43 (2010) 5163–5176.
[29] N.B. McKeown, P.M. Budd, Polymers of intrinsic microporosity (PIMs): organic materials for membrane separations, heterogeneous catalysis and hydrogen storage, Chem. Soc. Rev. 35 (2006) 675–683.
[30] Y. Wang, N.B. McKeown, K.J. Msayib, G.A. Turnbull, I.D.W. Samuel, Laser chemosensor with rapid responsivity and inherent memory based on a polymer of intrinsic microporosity, Sensors 11 (2011) 2478–2487.
[31] D.P. He, D.S. He, J.L. Yang, Z.X. Low, R. Malpass-Evans, M. Carta, N.B. McKeown, F. Marken, Molecularly rigid microporous polyamine captures and stabilizes conducting platinum nanoparticle networks, ACS Appl. Mater. Interfaces 8 (2016) 22425–22430.
[32] Y.Y. Rong, D.P. He, R. Malpass-Evans, M. Carta, N.B. Mckeown, M.F. Gromboni, L.H. Mascaro, G.W. Nelson, J.S. Foord, P. Holdway, S.E.C. Dale, S. Bending, F. Marken, High-utilisation nanoplatinum catalyst (Pt@cPIM) obtained via vacuum carbonisation in a molecularly rigid polymer of intrinsic microporosity, Electrocatalysis 8 (2017) 132–143.
[33] H.J. Kim, D.G. Kim, K. Lee, Y. Baek, Y. Yoo, Y.S. Kim, B.G. Kim, J.C. Lee, Carbonaceous membrane based on a polymer of intrinsic microporosity (PIM-1) for water treatment, Sci. Rep. 6 (2016) 36078.
[34] P.M. Budd, K.J. Msayib, C.E. Tattershall, B.S. Ghanem, K.J. Reynolds, N.B. McKeown, D. Fritsch, Gas separation membranes from polymers of intrinsic microporosity, J. Membr. Sci. 251 (2005) 263–269.
[35] M. Carta, R. Malpass-Evans, M. Croad, Y. Rogan, J.C. Jansen, P. Bernardo, F. Bazzarelli, N.B. McKeown, An efficient polymer molecular sieve for membrane gas separations, Science 339 (2013) 303–307.
[36] M. Carta, R. Malpass-Evans, M. Croad, Y. Rogan, M. Lee, I. Rose, N.B. McKeown, Synthesis of cardo-polymers using Troger's base formation, Polym. Chem. 5 (2014) 5267–5272.
[37] A.C. Ferrari, Raman spectroscopy of graphene and graphite: disorder, electron–phonon coupling, doping and nonadiabatic effects, Solid State Commun. 143 (2007) 47–57.
[38] V.Y. Osipov, A.V. Baranov, V.A. Ermakov, T.L. Makarova, L.F. Chungong, A.I. Shames, K. Takai, T. Enoki, Y. Kaburagi, M. Endo, A.Y. Vul, Raman characterization and UV optical absorption studies of surface plasmon resonance in multishell nanographite, Diam. Rel. Mater. 20 (2011) 205–209.
[39] C. Hu, S. Sedghi, A. Silvestre-Albero, G.G. Andersson, A. Sharma, P. Pendleton, F. Rodríguez-Reinoso, K. Kaneko, M.J. Biggs, Raman spectroscopy study of the transformation of the carbonaceous skeleton of a polymer-based nanoporous carbon along the thermal annealing pathway, Carbon 85 (2015) 147–158.
[40] P.K. Chu, L.H. Li, Characterization of amorphous and nanocrystalline carbon films, Mater. Chem. Phys. 96 (2006) 253–277.
[41] E. Madrid, Y.Y. Rong, M. Carta, N.B. McKeown, R. Malpass-Evans, G.A. Attard, T.J. Clarke, S.H. Taylor, Y.T. Long, F. Marken, Metastable ionic diodes derived from an amine-based polymer of intrinsic microporosity, Angew. Chem. Int. Ed. 53 (2014) 10751–10754.